Available online at www.sciencedirect.com
SCIENCE DIRECT®
International Journal of Thermal Sciences 44 (2005) 429–440
International Journal of Thermal Sciences
www.elsevier.com/locate/ijts

Effects of gravity on structure and entropy generation of confined laminar diffusion flames

A. Datta [1]

Department of Power Engineering, Jadvapur University, Salt Lake Campus, Kolkata 700098, India

Received 26 October 2004; accepted 26 October 2004

Abstract

A numerical prediction of a confined, co-flowing, laminar jet diffusion flame has been made to find the flow and scalar variables under steady state condition. These variables are used for the description of the flame structure and the evaluation of entropy generation rate and the rate of exergy loss. The exergy loss is compared against the exergy coming in, to evaluate the second law efficiency of the combustion process. The model is applied for diffusion flames in a confined geometry at various gravity levels to find the effect of gravity on the rate of entropy generation and second law efficiency. In general, the flame becomes wider in shape at reduced gravity. A correlation of the flame width against Froude number over a wide gravity range has been proposed. It is observed from the local volumetric entropy generation rate that a diffusion flame is more intense at its base than at the tip. The intensity of the flame becomes less at reduced gravity because of the lower rate of entrainment of oxygen. The entropy generation rate due to heat transfer increases considerably at normal gravity compared to that at zero gravity, because of the thermal stratification of the flow under the influence of buoyant acceleration. The rate of entropy generation due to chemical reaction and mass transfer remain almost unaltered at all gravity levels. The lowering of the total entropy generation rate and the corresponding exergy destruction increases the second law efficiency of a confined diffusion flame at reduced gravity compared to that at normal gravity.

Keywords: Diffusion flame; Exergy; Entropy generation; Gravity

1. Introduction

Laminar jet diffusion flame, involving gaseous fuel, is one of the fundamental types of flame studied in combustion and has a very important role in energy research. Diffusion flames have widespread use in practical burners, furnaces and combustors, used for energy conversion. Though, most of the diffusion flames employed in practice are turbulent, laminar diffusion flames have never lost their importance as they are better tractable, both theoretically and experimentally, than their turbulent counterparts. Moreover, understanding the transport and reaction processes in a laminar diffusion flame serves as a necessary precursor for understanding the structure of the more complicated turbulent flames. In many cases, the turbulent flames are studied through the laminar flamelet concept, establishing a direct correspondence between the two flame types.

In the earth's atmosphere the structure of a low velocity diffusion flame is profoundly affected by gravity. However, with the increase in the jet velocity the effect of gravity diminishes, and the turbulent diffusion flames can often be treated as non-buoyant, even at normal gravity. Therefore, a concern in the study of laminar diffusion flames under normal gravity is the disturbance due to the buoyancy and its effect on the flame behaviour. Studying combustion at no-gravity or micro-gravity can seclude this influence. Combustion study in micro-gravity is further important for fire safety in space-crafts and rockets where combustion occurs at different gravity levels.

Law and Faeth [1] reviewed the earliest works on the effects of gravity on various flame characteristics including

E-mail address: amdatta@hotmail.com (A. Datta).
[1] Phone : +91 33 23355813, fax : +91 33 23357254.

1290-0729/$ – see front matter
doi:10.1016/j.ijthermalsci.2004.10.003

Nomenclature

A	pre-exponential number
A_{in}	rate of incoming exergy ..... W
C_j	concentration (mass fraction) of the jth species
c_p	specific heat ..... $\text{J}\cdot\text{Kg}^{-1}\cdot\text{k}^{-1}$
d_f	fuel jet diameter ..... m
D_{jm}	mass diffusivity of jth species in a binary mixture of j and N_2 ..... $\text{m}^2\cdot\text{s}^{-1}$
$\dot{e}_g$	volumetric entropy generation rate $\text{W}\cdot\text{m}^{-3}\cdot\text{K}^{-1}$
E	activation energy ..... $\text{J}\cdot\text{kmol}^{-1}$
$\dot{E}_g$	entropy generation rate ..... $\text{W}\cdot\text{K}^{-1}$
Fr	Froude number (u_f^2/gd_f)
g	acceleration due to gravity ..... $\text{m}\cdot\text{s}^{-2}$
g_n	acceleration due to normal gravity, $= 9.81\ \text{m}\cdot\text{s}^{-2}$
h	enthalpy ..... J
$\dot{I}$	rate of exergy destruction/irreversibility .... W
Le_j	Lewis number of jth species
L_f	flame height or length ..... m
M	molecular weight
p	pressure ..... $\text{N}\cdot\text{m}^{-2}$
Pr	Prandtl number
S_{cj}	rate of production of species j per unit volume ..... $\text{kg}\cdot\text{m}^{-3}\cdot\text{s}^{-1}$
r	radial distance ..... m
$\overline{R}$	universal gas constant
T	temperature ..... K
T_o	exergy reference temperature, $= 298$ K
t	time ..... s
u_f	fuel jet velocity ..... $\text{m}\cdot\text{s}^{-1}$
v	velocity ..... $\text{m}\cdot\text{s}^{-1}$
w	flame width ..... m

Greek symbols

ρ	density ..... $\text{kg}\cdot\text{m}^{-3}$
μ	viscosity ..... $\text{kg}\cdot\text{m}^{-1}\cdot\text{s}^{-1}$
λ	thermal conductivity ..... $\text{W}\cdot\text{m}^{-1}\cdot\text{K}^{-1}$
ω	reaction rate ..... $\text{kmol}\cdot\text{m}^{-3}\cdot\text{s}^{-1}$
η_{II}	second law efficiency

Subscripts

j	species identification
k	identification of the reaction step
r	radial direction
z	axial direction

diffusion flames. The main thrust of microgravity research was on flame structure, stability and soot emission from diffusion flames. The earliest microgravity tests were conducted in drop towers. It was observed that as the gravity level reduced from normal value, the flame length first decreased during a transient phase and then gradually lengthened toward the steady non-buoyant configuration. The results from different tests on flame height at reduced gravity was not very conclusive as both increase and decrease of flame height are reported as the gravity level was reduced. However, it is universally concluded that the flame widens remarkably with the reduction in gravity level. At zero gravity and for negligible jet momentum, diffusion is equally probable in all directions and a spherical diffusion flame is obtained. As the jet momentum is increased the flame length increases at all gravity levels and finally the transition from laminar to turbulent flame takes place. Lin et al. [2] found the normalized flame width (wZ_{st}/d_f) to be a constant value, where Z_{st} is the stoichiometric mixture fraction. Davis et al. [3] argued that Froude number is the appropriate scaling parameter for gravitational variation in laminar jet diffusion flames. Extensive studies on the effect of gravity on diffusion flame width are reported by Sunderland et al. [4]. They have correlated the flame width against Froude number in the form $(w/d_f) = X(Fr)^y$ where X and y are constants and are different for different fuels.

In addition to the physical structures, the flame stability and emission characteristics are also affected by gravity. Observation with the candle flames show that for the same conditions the burning rate per unit wick surface area were considerably reduced at reduced gravity levels (Ross et al. [5]). This is due to the absence of buoyancy driven flow, which serves to transport the oxygen and drive away the products from the flame zone at a faster rate. The absence of the buoyancy induced flow in micro-gravity environment results in an increase in the reactant residence time, which alters the processes like stability, radiation, soot formation and soot oxidation in the flame. Maruta et al. [6] studied the extinction of counterflow diffusion flame at microgravity. They obtained a C-shaped extinction curve by plotting the stretch rates against fuel concentration limits, indicating two kinds of extinctions. They identified those as the stretch extinction and radiation extinction. Atreya and Agrawal [7] also showed radiative extinction of diffusion flames in quiescent micro-gravity environments. Ezekoye and Zhang [8] modeled the soot oxidation and agglomeration in diffusion flames at micro-gravity.

One area of combustion science, which has received relatively less attention, is the thermodynamics of the flame. During combustion of fuel, complex transport and chemical processes take place simultaneously, resulting in the release of chemical energy in the form of heat and distribution of the thermal energy as a result of advective and diffusive transports. All the processes involved are irreversible and results in the destruction of exergy stored in the fuel. This should have very important implications in work-producing devices, like engines, where loss of exergy during combustion means loss of useful work potential of the fuel. Keenan [9]

was first to recognize that the energy efficiency of a device does not always reflect the true cost of an industrial process and the true cost is better reflected by exergy or available energy. The loss of exergy can be estimated by the Gouy Stodola theorem (Bejan [10]), which relates the rate of exergy destruction with the rate of entropy generation in the process. It is, therefore, important to identify the principal routes of entropy generation in flames and to evaluate their relative weights at different conditions.

Arpaci and Selamet [11] studied the entropy production in premixed flames from a flat flame burner. The entropy generation rate expression in their analysis contained contributions due to dissipation of thermal energy, mechanical energy and other forms of energy. A non-dimensional entropy generation rate expression was defined and was found to be an inverse function of the square of the Peclet number. From this, the authors found that the minimum quench distance for the flame corresponds to an extremum condition in the entropy production. San et al. [12] reported an expression of volumetric entropy generation rate for a Newtonian fluid for reacting flow and with heat and mass transport following Hirschfelder et al. [13]. The work of San et al., however, was restricted to combined heat and mass transfer only, without any involvement of chemical reaction.

Puri [14] and Hiwase et al. [15] studied the second law analysis for single droplet burning. Puri [14] obtained an optimum transfer number for minimizing entropy generation in droplet combustion. The optimum transfer number is observed to be directly proportional to the square of the relative velocity and inversely proportional to the heat release rate and the temperature difference between the droplet and the surrounding flow. Hiwase et al. [15] developed a theoretical model of exergy analysis of droplet combustion as a function of Damkohler number and initial droplet temperature. Datta and Som [16] evaluated the rate of exergy loss and the second law efficiency in a spray combustion process under different operating conditions, like inlet pressure, temperature, swirl and drop characteristics in the atomized fuel spray.

Datta [17] evaluated the rate of entropy generation in a laminar jet diffusion flame. The work revealed that in diffusion flames the main contributor of entropy generation is the heat transport processes. The chemical reaction rate also has a significant contribution towards entropy generation in diffusion flame, but it is much smaller than that by heat transfer. The other transports have much less contribution towards entropy generation. It was found that the increase in the air temperature in a diffusion flame reduces the rate of entropy generation, while a decrease in the air-fuel ratio increases the rate of entropy generation in diffusion flames. Nishida et al. [18] analyzed the local entropy generation and exergy loss in premixed and diffusion flames. The dominant process of exergy loss in the premixed flame is reported to be the chemical reaction. However, for the diffusion flames, Nishida et al. corroborated the earlier finding of Datta [17] that the main contribution towards entropy generation comes from the heat transport.

Both the diffusion flame analysis of Datta [17] and Nishida et al. [18] were carried out at normal gravity with laminar diffusion flames, where the buoyancy takes a major role in defining the flow and transport processes. At reduced and no gravity, the buoyancy induced motion will be absent. This may significantly alter the entropy production rate as well. As buoyancy has almost no role in practical combustion processes, the exergy analysis for the practical combustors will be better explained by analyzing diffusion flames under the microgravity conditions. The present work has studied the structure, entropy generation and exergy loss in a co-flow, laminar, gaseous, jet diffusion flame at normal gravity as well as at various reduced gravity levels within a confined geometry. The flame conditions are taken as the same as that in the earlier work of Datta [17]. The numerical model adopted for the analysis is, however, improved from the earlier one. The present model adopted two step reaction kinetics of methane fuel instead of the single step adopted earlier. The variations in the thermodynamic and transport properties based on local temperature and species concentrations are considered. The gravity level is reduced from the normal value gradually up to zero. The numerical model for the reacting flow is first solved for the development of the steady state conditions and then the steady state variables are used in the entropy generation rate expression to evaluate the rate of entropy generation. The rate of exergy loss is computed and compared against the inlet exergy to find out the second law efficiency of the combustion process.

2. Model formulation

The laminar diffusion flame in a confined physical environment is considered with fuel (methane) admitted as a central jet and air as a co-flowing annular jet (Fig. 1). The inner fuel tube diameter is 0.0127 m and the outer tube diameter is 0.0504 m. The inner tube is considered to be thin and its thickness is neglected for the computation. The length of the confined domain is taken as 0.3 m. The dimensions are in conformity with the earlier experimental work of Mitchell et al. [19] and the numerical work of Smooke et al. [20]. Considering the axi-symmetric geometry, the numerical simulation domain is considered on one side of the axis only (shown by the dotted lines in Fig. 1).

The combustion process is simulated by employing a detailed numerical model, solving the governing equations for a laminar, axi-symmetric, reacting flow with appropriate boundary conditions. The flow is vertical through the reaction space and the gravity effect is included in the axial momentum equation. The conservation equations for mass and momentum are as follows:

Mass:

$$\frac{\partial \rho}{\partial t} + \frac{1}{r}\frac{\partial}{\partial r}(r\rho v_r) + \frac{\partial}{\partial z}(\rho v_z) = 0 \tag{1}$$

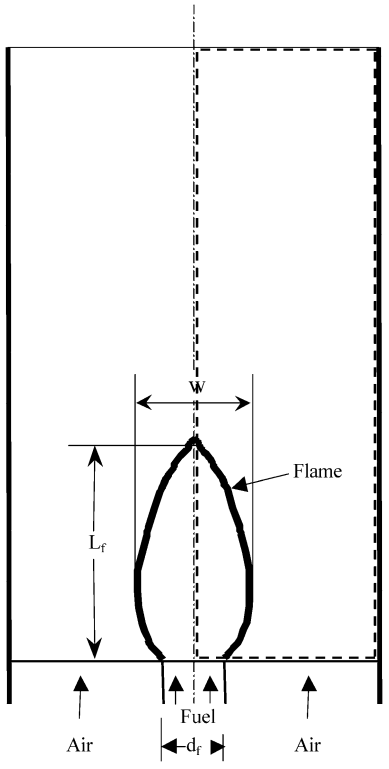

Fig. 1. Physical model: Schematic of the geometry and flame. The dotted lines encompass the computational domain.

Radial momentum:

$$\frac{\partial}{\partial t}(\rho v_r) + \frac{1}{r}\frac{\partial}{\partial r}\left(r\rho v_r^2\right) + \frac{\partial}{\partial z}(\rho v_r v_z) = -\frac{\partial p}{\partial r} + \frac{2}{r}\frac{\partial}{\partial r}\left(r\mu\frac{\partial v_r}{\partial r}\right) - \frac{2}{r}\mu\frac{v_r}{r^2} + \frac{\partial}{\partial z}\left\{\mu\left(\frac{\partial v_z}{\partial r} + \frac{\partial v_r}{\partial z}\right)\right\} - \frac{2}{3}\frac{\partial}{\partial r}\left(\mu\left(\frac{\partial v_r}{\partial r} + \frac{v_r}{r} + \frac{\partial v_z}{\partial z}\right)\right) \quad (2)$$

Axial momentum:

$$\frac{\partial}{\partial t}(\rho v_z) + \frac{1}{r}\frac{\partial}{\partial r}(r\rho v_r v_z) + \frac{\partial}{\partial z}\left(\rho v_z^2\right) = -\frac{\partial p}{\partial z} + \frac{1}{r}\frac{\partial}{\partial r}\left\{r\mu\left(\frac{\partial v_z}{\partial r} + \frac{\partial v_r}{\partial z}\right)\right\} + 2\frac{\partial}{\partial z}\left(\mu\frac{\partial v_z}{\partial z}\right) - \frac{2}{3}\frac{\partial}{\partial z}\left\{\mu\left(\frac{\partial v_r}{\partial r} + \frac{v_r}{r} + \frac{\partial v_z}{\partial z}\right)\right\} + \rho g \quad (3)$$

In the axial momentum equation, 'g' represents the acceleration due to gravity. At normal gravity, the value of g is 9.81 m·s^{-2}. This is reduced at reduced gravity levels and will come to zero at zero gravity.

The combustion reaction of methane and air is assumed to proceed through two step global reaction chemistry as

$$CH_4 + 1.5O_2 \rightarrow CO + 2H_2O \quad (4)$$

$$CO + 0.5O_2 \rightarrow CO_2 \quad (5)$$

The reaction rates for the above reactions are obtained following an Arrhenius type rate equation, given as

$$\omega = A\rho^{(a+b)}\frac{C_1^a C_2^b}{M_1^a M_2^b}\exp\left(-\frac{E}{\overline{R}T}\right) \quad (6)$$

where, A and E are the pre-exponential factor and activation energy, respectively, for the respective equations and a and b are the reaction orders in terms of fuel and oxygen respectively. The values for these parameters are taken from the work of DuPont et al. [21].

The conservation equation for chemical species is solved for five species, viz. CH_4, O_2, CO_2, CO and H_2O. The concentration for the sixth species N_2 is obtained by difference. The governing equation for the species conservation is as follows:

$$\frac{\partial}{\partial t}(\rho C_j) + \frac{1}{r}\frac{\partial}{\partial r}(r\rho v_r C_j) + \frac{\partial}{\partial z}(\rho v_z C_j) = \frac{1}{r}\frac{\partial}{\partial r}\left(r\rho D_{jm}\frac{\partial C_j}{\partial r}\right) + \frac{\partial}{\partial z}\left(\rho D_{jm}\frac{\partial C_j}{\partial z}\right) + \dot{S}_{cj} \quad (7)$$

where, C_j is the mass fraction of the jth species. D_{jm} is the diffusion coefficient of the species in a binary mixture of that species and nitrogen (following Katta et al. [22]). The source term S_{cj} is the rate of production or destruction of the species j per unit volume due to chemical reaction. The source terms are calculated as

$$\dot{S}_{cj} = \sum_{k=1}^{2}\left(\gamma''_{jk}\dot{\omega}_k - \gamma'_{jk}\dot{\omega}_k\right)M_j \quad (8)$$

where, M_j is the molecular weight of the jth species. γ''_{jk} and γ'_{jk} are the stoichiometric coefficients on the product side and reactant side respectively for the jth species in the kth reaction. Obviously, for the present simple reaction mechanism, k is either 1 for the reaction given by Eq. (4) or (2) for the reaction given by Eq. (5).

The density of the species mixture is calculated using the equation of state considering all the species as ideal gases. The enthalpy for chemically reacting flows is given as the weighted sum of each mass fraction

$$h = \sum_{j=1}^{n} C_j h_j = \sum_{j=1}^{n} C_j\left(h_{fj}^0 + \int_{T_o}^{T} c_{pj}\,\mathrm{d}T\right) \quad (9)$$

where, h_{fj}^0 is the heat of formation of the jth species at the reference temperature T_0 and the integral part is the contribution of the sensible heat.

The energy equation is written as

$$\frac{\partial}{\partial t}(\rho h) + \frac{1}{r}\frac{\partial}{\partial r}(r\rho v_r h) + \frac{\partial}{\partial z}(\rho v_z h) = \frac{1}{r}\frac{\partial}{\partial r}\left(r\frac{\lambda}{c_p}\frac{\partial h}{\partial r}\right) + \frac{\partial}{\partial z}\left(\frac{\lambda}{c_p}\frac{\partial h}{\partial z}\right) + \frac{1}{r}\frac{\partial}{\partial r}\left[r\frac{\lambda}{c_p}\sum_{j=1}^{n} h_j\left(Le_j^{-1} - 1\right)\frac{\partial C_j}{\partial r}\right]$$

$$+\frac{\partial}{\partial z}\left[\frac{\lambda}{c_p}\sum_{j=1}^{n}h_j\left(Le_j^{-1}-1\right)\frac{\partial C_j}{\partial z}\right] \tag{10}$$

Le_j in the above equation is the local Lewis number of the jth species defined as

$$Le_j=\frac{\lambda}{c_p}\frac{1}{\rho D_{jm}} \tag{11}$$

The last two terms in the enthalpy equation (10) are caused by the preferential diffusion of species in the radial and axial directions respectively. The Soret effect, caused by the thermal-diffusion effect, is neglected in the present analysis. The present analysis also neglects the radiative exchange of energy in the flame considering the non-sooty behaviour of the methane flame. The specific heat c_p is a strong function of temperature and is locally calculated for each species at the respective temperature. The mixture specific heat is then calculated considering an ideal gas mixture. The temperature of the gas mixture is implicitly calculated by solving Eq. (9) using a Newton–Raphson method. The solution is refined until the accuracy within the prescribed criteria is achieved.

2.1. Evaluation of transport properties

The transport of momentum, energy and species mass in the calculation of a reacting flow involve the transport coefficients like viscosity (μ), thermal conductivity (λ) and mass diffusivity (D_{jm}) for the solution. In a multi-component mixture, such as here, the evaluation of the transport properties requires some model. In the present work, a detailed evaluation of the transport properties is considered.

The local viscosity of the species j is computed from the local temperature using a power law as

$$\mu_j=\mu_j^0\left(\frac{T}{T_0}\right)^p \tag{12}$$

μ_j^0 represents the reference viscosity of species j at the reference temperature T_0. The exponent p is taken as 0.7 (Smooke et al. [20]). The viscosity of the mixture is calculated using the semi-empirical method of Wilke, as described in Reid et al. [23].

The local thermal conductivity of species j is evaluated using a polynomial expression of thermal conductivity of pure substance as

$$\lambda_j=A_j+B_jT+C_jT^2+D_jT^3 \tag{13}$$

where, A_j, B_j, C_j, and D_j are the coefficients for species j which are taken from Reid et al. [23]. The mixture thermal conductivity is again evaluated using the method of Wilke. The mass diffusivity, D_{jm}, for species j in a binary mixture of j and nitrogen is evaluated using a power law like (Turns [24])

$$D_{jm}=D_{jm}^0\left(\frac{T}{T_0}\right)^{1.5} \tag{14}$$

2.2. Boundary conditions

Boundary conditions for the governing equations are defined at inlet, outlet, axis and at the wall. At the inlet, the boundary conditions are given separately for the fuel stream at the central jet and the air stream at the annular co-flow. The streams are considered to enter the computational domain as plug flow, with velocities calculated from their respective flow rates. The temperatures of fuel and air are specified. In conformation with the conditions used by Mitchell et al. [19], and Smooke et al. [20], the fuel jet velocity is taken as 4.5 $\mathrm{cm\cdot s^{-1}}$ and the air jet velocity as 9.88 $\mathrm{cm\cdot s^{-1}}$. The temperatures for both the streams are 298 K.

Considering the length of the computational domain to be 0.3 m, the fully developed boundary conditions for the variables are considered at the outlet. In case of reverse flow at the outlet plane, which occurs in the case of buoyant flame, the stream coming in from the outside is considered to be air.

Axi-symmetric condition is considered at the central axis, while at the wall a no-slip, adiabatic and impermeable boundary condition is adopted.

2.3. Exergy model

The entropy generation rate due to the transport of heat, mass and momentum along with the chemical reaction is determined from the general entropy transport equation. The entropy generation rate per unit volume, $\dot{e}_g$, at a point in the gas phase can be written in the tensorial notation, following San et al. [12] as,

$$\begin{aligned}\dot{e}_g=&\frac{\Delta:\sigma}{T}+\frac{-J^q\nabla T}{T^2}\\&+\frac{\sum_j(J_j^m\nabla\alpha_j^c)}{T}+\frac{\sum_j(-s_jJ_j^m\nabla T)}{T}\\&+\frac{1}{T}\sum_k\sum_j\left(\gamma'_{jk}-\gamma''_{jk}\right)\alpha_j^c\dot{\omega}_k\end{aligned} \tag{15}$$

where, σ and Δ are the stress ($\mathrm{N\cdot m^{-2}}$) and rate of strain ($1\cdot\mathrm{s^{-1}}$) tensors respectively, J^q is the heat flux per unit area ($\mathrm{W\cdot m^{-2}}$) and J_j^m, α_j^c and s_j are the mole flux per unit area ($\mathrm{kmol\cdot m^{-2}\cdot s^{-1}}$), chemical potential ($\mathrm{J\cdot kmol^{-1}}$) and partial molal entropy of the jth species ($\mathrm{J\cdot kmol^{-1}\cdot K^{-1}}$), respectively. γ'_{jk} and γ''_{jk} are the stoichiometric coefficients on the reactant side and product side, respectively, for the jth species in the kth reaction, and ω_k is the reaction rate of the kth reaction. The first term on the right-hand side of Eq. (15) is due to fluid friction (momentum transfer), the second term is due to heat transfer, the third term pertains to mass transfer, the fourth term arises from the coupling between heat and mass transfer and the fifth term is due to chemical reaction. The fifth term has summation over all the species and for all the reactions. The entropy generation due to body force is neglected in the above equation, because it is small even at normal gravity level compared to the other entropy generation terms for reacting flows [12].

Carrington and Sun [25] studied the terms of the above Eq. (15) elaborately and came to the conclusion that the entropy generation term due to coupled heat and mass transfer vanishes and does not make any contribution unless the Soret and Dufour effects have significant influence. The analysis of Puri [14] corroborates this finding. In the present analysis Soret and Dufour effects are neglected compared to direct heat and mass diffusion. Therefore, the coupling term is not taken into consideration while calculating the entropy generation rate in the flame and the four other terms of Eq. (15) are only considered.

Each term of Eq. (15) is expanded in a cylindrical coordinate system to determine $\dot{e}_g$, with the velocity, temperature and concentration values calculated from the numerical computation of the diffusion flame solving the respective governing equations as explained before. The total entropy generation is calculated as

$$\dot{E}_g = \iiint_{\forall} \dot{e}_g \, \mathrm{d}\forall \tag{16}$$

where, $\forall$ is the volume of the domain of interest in which all the physical and chemical processes take place.

The rate of irreversibility (i.e., exergy loss) in the combustion process is found out using the Gouy Stodola theorem, as,

$$\dot{I} = T_o \dot{E}_g \tag{17}$$

The second law efficiency is defined as the fraction of the incoming exergy lost during the process. The incoming exergy is associated only with fuel (chemical exergy), as the inlet air is at exergy reference temperature (298 K). The specific exergy of methane is taken as 890.3 kJ·mol^{-1} and is multiplied by the fuel flow rate to find the rate of exergy coming in (A_{in}). The second law efficiency is given by

$$\eta_{\mathrm{II}} = 1 - \frac{\dot{I}}{A_{\mathrm{in}}} \tag{18}$$

3. Numerical scheme

The gas phase conservation equations of mass (Eq. (1)), momentum (Eqs. (2) and (3)), energy (Eq. (10)) and species concentrations (Eq. (7)) are solved simultaneously with their appropriate boundary conditions by an explicit finite difference computing technique following a modified version of the SOLA algorithm developed by Hirt and Cook [26]. The model was earlier adopted by Datta [17] for the solution of the laminar diffusion flames. The variables are defined following a staggered grid arrangement. The advection terms are discretised following a hybrid differencing scheme, based on cell Peclet number, while the diffusion terms are discretised by the central differencing scheme. At first, the axial and radial momentum equations are solved. Pressure corrections and the associated corrections of velocities to satisfy the conservation of mass are then done by an iterative scheme. The enthalpy transport and the species transport equations are subsequently solved. The temperature is decoded from the enthalpy and species concentration values by Newton–Raphson method. The solution is explicitly advanced in time till a steady state convergence is achieved. The time increment for the explicit advancement is done satisfying the stability criteria and the condition that a fluid particle should never cross a complete cell, in either direction, in one time step.

The combustion is simulated by increasing the temperature of a few cells a little above the burner tip and at the interface of the two jets. This criterion, simulating the spark, is withdrawn once the flame has been established. After the flame is ignited, the time steps are kept further reduced to avoid divergence of the results due to the increased source terms. The flame at normal gravity is first solved. The steady state values for this condition are then used for the starting conditions for the next lower gravity level. This process is continued till a steady solution at zero gravity level is achieved.

A variable size adaptive grid system is considered with higher concentration of nodes near the axis, where larger variations of the variables are expected. However, the variations in the size of the grids are ensured to be gradual. Grid testing is done by several variations of the number of grids in either direction. It is observed that the increase in the numbers of grids from 85×41 to 121×61 almost doubles the computation time, but the maximum change in results is within 2%. Hence a numerical mesh with 85×41 grid nodes is finally adopted.

4. Results and discussion

At first, a validation of the present numerical code has been made by comparing its predictions with the experimental results of Mitchell et al. [19], for the same operating conditions. Fig. 2 shows the predicted and measured radial

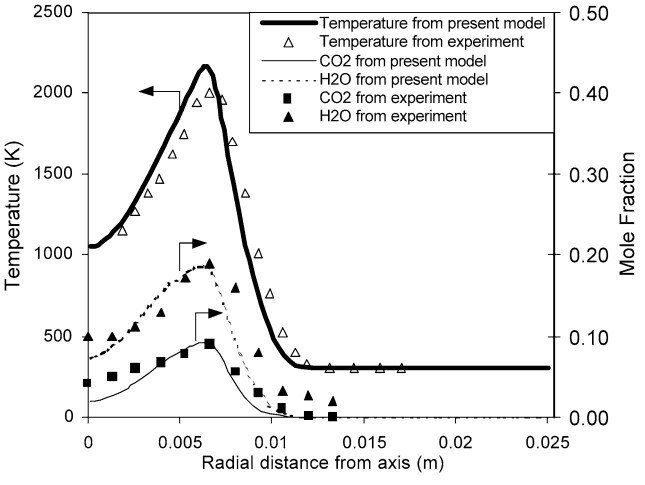

Fig. 2. Comparison of the radial distributions of temperature and CO_2 and H_2O concentrations predicted by the present model against the experimental data of Mitchell et al. [19] at 12 mm above burner and at normal gravity.

distributions of temperature and the product species concentrations (CO_2 and H_2O), respectively, at an axial height of 12 mm above the burner. The temperature data show excellent agreement. The increase of temperature and its subsequent decay from the axis towards the periphery as well as the peak temperature are well predicted. However, the present code predicts the flame a little closer (by 0.3 mm) to the axis compared to that from the experiments. The species distributions of the combustion products also show reasonably good agreement. It is observed from the figure that at the axis the predicted concentrations of the species are less than the measured values. But the peak concentrations correspond very well both in terms of magnitude and location. The results establish the predictive capability of the present calculation method for the type of flame studied.

Fig. 3(a) and (b) illustrate the diffusion flame structures at normal and zero gravity respectively. In these figures the velocity field, temperature distribution and the flame front are simultaneously presented. In the figures the radial axes are stretched to improve the clarity of the presented results. The flame front is drawn by drawing the contour of the non-dimensional volumetric energy release rate of value 0.001. The energy release rate is non-dimensionalised by its maximum value for the corresponding condition. It means that the volumetric energy release rates at all points outside the flame front, shown in the figures, are less than 0.1% of the maximum volumetric heat release rate, and can be neglected. Therefore, heat releases only in the marked zone, which is depicted as the flame. The wiggles in the flame fronts, seen in the figures, do not actually exist and are the results of stretching of the radial axes. It is observed from the figures that in both the cases burner stabilized flames are achieved. Initially some flow entrainment takes place from the co-flowing air towards the central jet due to momentum transfer. This entrainment along with the diffusion of gases into each other result in the formation of the flammable fuel-air mixture at an interface. The burning initiates in the flammable mixture and raises the temperature of the product gas. In the presence of gravity, this results in an acceleration of flow helped by buoyancy. It is reflected by the bigger velocity vectors in the normal gravity flame shown in Fig. 3(a). The high velocity central flow entrains air from the co-flow at an increased rate. As a result the flame front itself turns inward and takes an elongated shape. The high temperature gas moves towards the core and flows up through the central portion. This results in a void near the periphery. Air from outside flows in to fill the void through the exit plane, resulting in a recirculating zone around the periphery. The flow velocity in the recirculating mass is, however, low and it primarily forms a low temperature shield around the outer wall. The highest temperature zone is observed to be within the flame front. Beyond the flame front a thermal stratification takes place, guided by the flow field, with the high temperature gas located near the core and low temperature around the periphery. Considering the height of the flame to be the middle of the reaction zone on the axis, the flame height is found to be 12 cm.

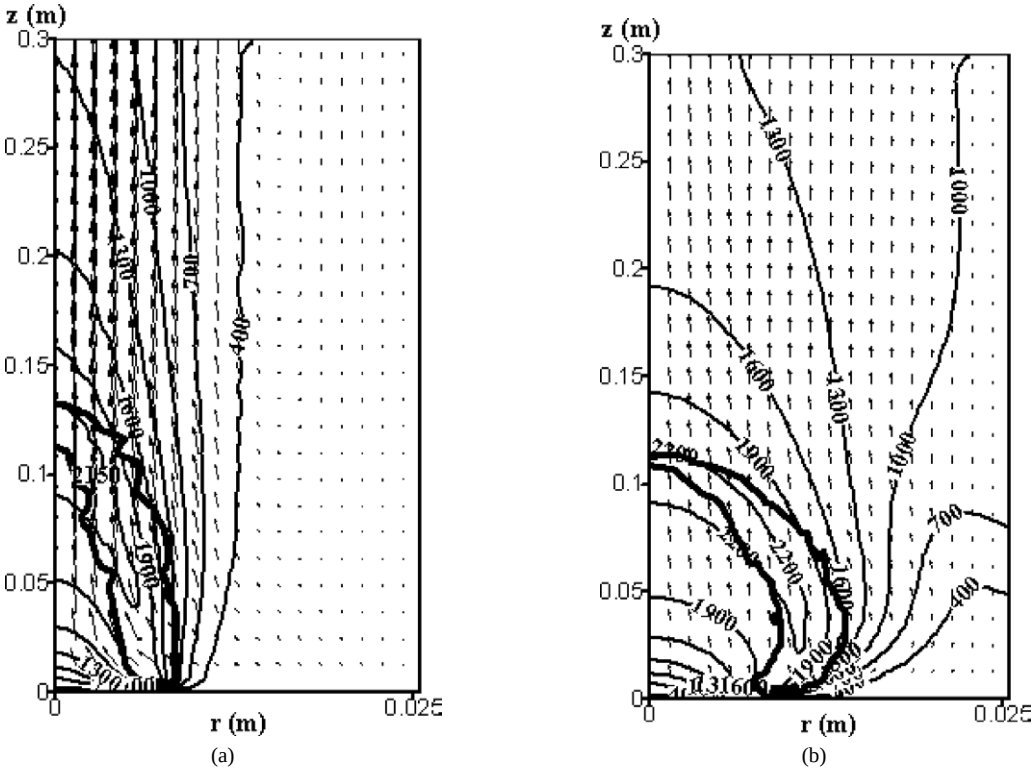

Fig. 3. (a) Flame (thick line), temperature distribution (contours in K) and velocity distribution (vectors) at normal gravity condition. (b) Flame (thick line), temperature distribution (contours in K) and velocity distribution (vectors) at zero gravity condition.

Fig. 3(b) depicts the flame at zero gravity. It is clearly evident from the figure that in the absence of gravity the flow is not accelerated to the extent as with the normal gravity. There is some initial entrainment due to the jet motion to form a flammable mixture, which gets ignited. However, with the increase in temperature following ignition the gas expands and flows outwardly in the absence of buoyancy. Therefore, the co-flowing air velocity vectors, a little above the inlet plane, are seen to have an outward direction. The flame front follows the flow-field and also turns away from the axis. Subsequently, the entrainment of flow towards the core results due to the increase in temperature of gas at the centre. This turns the flame inward and finally the flame meets at the axis at a certain height (∼10.9 cm). For the particular conditions adopted here, the height of the flame is somewhat reduced in the absence of gravity, however, the width increases considerably. The decrease in the flame height may be attributed to the reduced central flow velocity in the absence of gravity compared to that with gravity in a confined environment due to the absence of buoyancy and the peripheral recirculating zone.

The low velocity of flow in the absence of gravity increases the residence time of gas through the flame. The diffusion takes a dominant role in the absence of high axial velocity and the high temperature zone is more uniformly distributed in the entire domain. The temperature near the wall is high and no ingress is observed from the exit plane. Thus, a considerable variation in the velocity, temperature and flame structures are observed in the presence and absence of gravity.

Fig. 4 reports the flame profiles drawn by plotting the contour of the unity equivalence ratio for different gravity levels. The unity equivalence ratio line follows a trajectory through the middle of the flame contour shown earlier (Fig. 3(a) and (b)). The wiggles in the contour lines are again due to the stretching of the radial axis, which is maintained to distinctly separate the flame contours from one another. The flame contours at different gravity levels show that with the decrease in gravity, the flame continually widens while the flame height shortens only marginally. The width of the flames can be evaluated from the position of the maximum radial location of the flame contour.

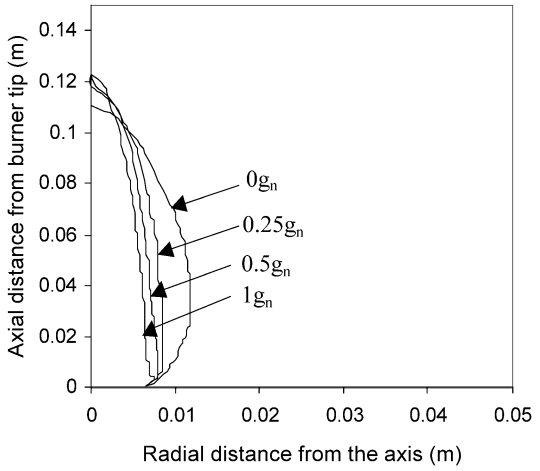

Fig. 4. Diffusion flame contours having equivalence Ratio $\phi = 1$ at different gravity levels.

It is observed that gravity has a profound effect on the diffusion flame width. Similar shape change was also reported in the earlier literature. Sunderland et al. [4] obtained correlations of flame width against Froude number for different hydrocarbons, viz. CH_4, C_2H_6 and C_3H_8. The correlation for methane was given as $(w/d_f) = 2.17Fr^{0.154}$. However, Sunderland et al., performed their experiments only at normal gravity and zero gravity conditions and did not provide any evidence whether the correlations apply at different intermediate gravity levels. Fig. 5(a) shows a plot of the non-dimensional flame width (w/d_f) against (Fr_n/Fr) obtained from the present numerical experiments. Fr_n is the Froude number with the normal gravity ($Fr_n = 0.016$). In varying

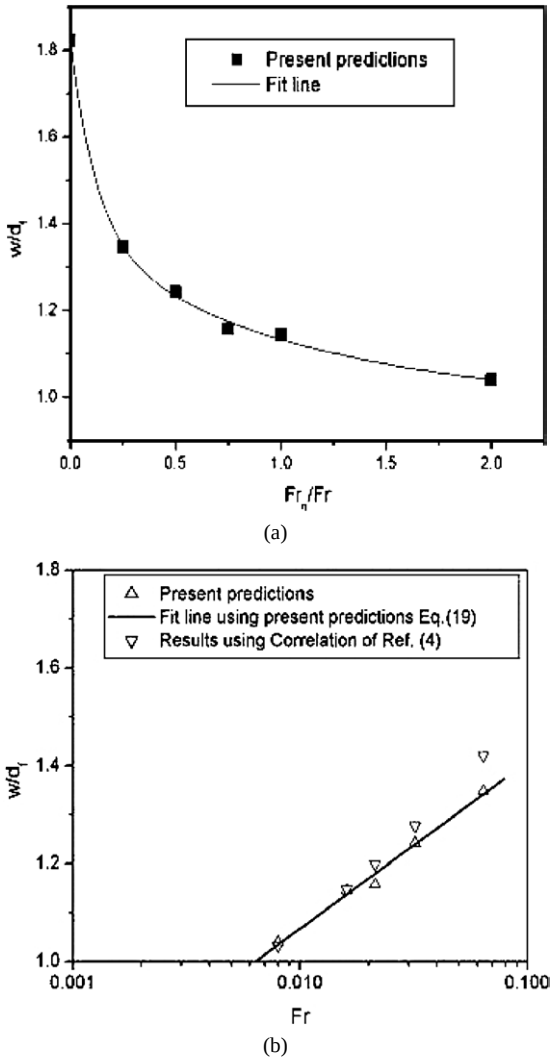

Fig. 5. (a) Plot of non-dimensional flame width against Froude number for various gravity levels. (b) Plot of non-dimensional flame width against Froude number in semi-logarithmic scale for various gravity levels to show the fit of Eq. (19) and comparison against empirical prediction of Ref. [4].

the Froude number (u_f^2/gd_f), only the gravity level (g) has been varied and the other quantities (i.e., u_f and d_f) are kept the same. Therefore, the ratio Fr_n/Fr represents the ratio of the actual gravitational level (g) to that at normal gravity (g_n). The actual gravity has been varied from 0 to $2g_n$ for the generation of the results. The curve in Fig. 5(a) shows a non-linear variation. To correlate the results of flame width against Froude number, similar in line to the correlations of Sunderland et al. [4], the results are plotted in a semi-logarithmic scale (except the one at zero gravity, which cannot be shown in log scale), as shown in Fig. 5(b). The data shown in the figure can be correlated by a linear fit as follows:

$$\frac{w}{d_f} = 2.08Fr^{0.146} \tag{19}$$

This correlation shows a very good agreement with the correlation obtained by Sunderland et al. [4] for methane. The values of the flame width obtained using the correlation of Sunderland et al. for the Froude numbers considered in the present case are also included in Fig. 5(b) for the sake of comparison. The ratio (w/d_f) predicted by the two correlations for the normal gravity flame with the present conditions differs by less than 1%. The result on the first hand establishes the predictions of the present model and on the second hand corroborate the flame width correlation at all gravity level.

The discussion that has been made so far revolves round the flame structure at various gravity levels. The other focus of this work is to investigate the effects of gravity on entropy generation and exergy destruction in diffusion flames. It may be pointed out here that a diffusion flame in a fully unconfined domain results in a complete loss of exergy if the dissipation process continues. The present work is, on the other hand, conducted in a confined environment to conform to practical situations in engines and combustors. The domain size is chosen sufficiently large compared to the flame front size, so that the effect of domain geometry on the thermodynamic parameters studied can become negligible. It has been detected from the exergy analysis that the fluid friction causes negligible generation of entropy compared to the other transport and chemical processes, viz. heat transfer, mass transfer and chemical reaction. Therefore, attention is given on these three modes of entropy generation individually. Fig. 6(a)–(c) illustrate the plots of the local volumetric entropy generation rate contours due to chemical reaction, heat dissipation and mass transfer, respectively, for the flame at normal gravity. In Fig. 6(a), the flame contour is also shown (as shown in Fig. 3(a)). Quite naturally, it is evident from the figure that the entropy generation due to chemical reaction takes place within the flame front. The volumetric entropy generation rate due to chemical reaction is higher near the base of the flame. It reveals that the flame is more intense near its base. At the tip, the flame is weak and the volumetric entropy generation rate is less than 1/20th of the peak contour value shown in the figure. The concentration gradient of the fuel is more at lower elevation and results in higher rate of diffusion of fuel towards the flame front. This makes the flame more intense there. With the consumption of fuel, the fuel concentration gradient reduces at higher elevation. This decreases the fuel

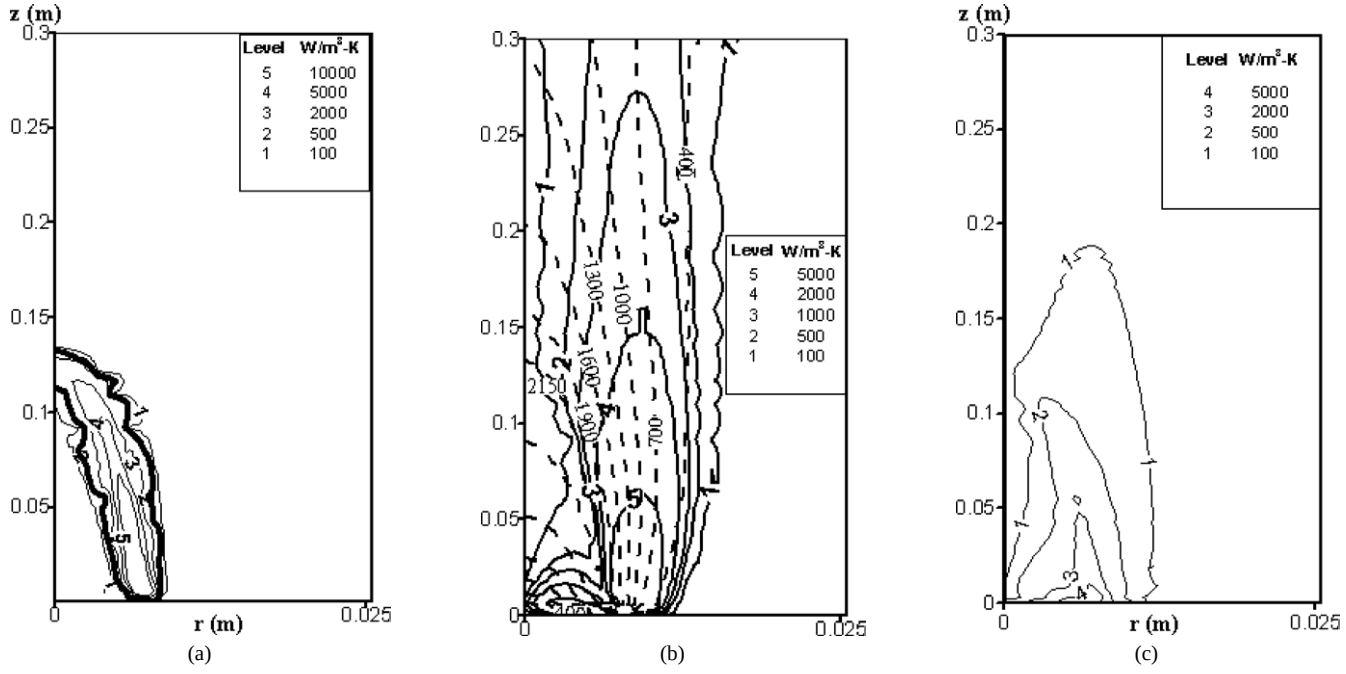

Fig. 6. (a) Flame front (thick line) and distribution of volumetric rate of entropy generation due to chemical reaction (solid contours) at normal gravity. (b) Temperature (in K) distribution (dotted contours) and the distribution of volumetric rate of entropy generation due to heat dissipation (solid contours) at normal gravity. (c) Distribution of volumetric rate of entropy generation due to mass transfer at normal gravity. The box insert in Fig. 6(a)–(c) show the values of the contour levels for the volumetric entropy generation rate.

transfer rate to the flame and the flame intensity also decreases.

Fig. 6(b) shows the volumetric entropy generation due to heat dissipation along with the temperature distribution in the confined domain. The strong temperature gradient close to the burner rim, where the flame is stabilized, increases the entropy generation there. The peak volumetric entropy generation rate due to heat dissipation is less than that due to chemical reaction. However, the entropy generation due to heat dissipation occurs over a much greater volume compared to the volume of the flame, where entropy generates due to chemical reaction. In the flame zone, heat dissipation occurs from the high temperature flame. Moreover, at normal gravity, the buoyancy-induced acceleration increases the flow velocity at the core and results in a high entrainment of fluid towards the centre. The flow structure generates a thermal stratification with the high temperature gas near the core. Due to the axi-symmetric nature of the flow the gradient of temperature remains low near the axis. The ingress of atmospheric air through the outlet plane and formation of the recirculation zone around the peripheral wall maintains a low temperature shield at the periphery. There exists an annular region between the core and the wall, where the temperature falls rapidly causing a high rate of heat dissipation. The stratification of the flow and the formation of the recirculating zone due to atmospheric air ingress maintain the annular region of high temperature gradient till the exit plane. Therefore, high dissipation of heat continues over a much larger volume to cause a high entropy generation.

The entropy generation due to mass transfer is depicted in Fig. 6(c) for the normal gravity condition. It is observed that the mass transfer results in entropy generation mainly around the flame. In a diffusion flame the reactants diffuse into the flame from the opposite sides of the flame surface and the products transport from the flame in all directions. Beyond the flame, though transport of heat continues, mass dissipation ceases to play any major role. The figure reveals that the magnitude of the rate of entropy generation per unit volume due to mass transfer is significantly lower compared to the other two major contributors even in the flame zone. Though generation and consumption of different species occur in the flame, the gradient of species concentrations never take a large value and the transport process always bring a uniformity in the distribution of the species around the flame. The only high rate of entropy generation due to mass transfer is observed just above the entry plane and around the interface between the fuel and air jets.

Fig. 7(a)–(c) show the similar figures for zero gravity, viz. the distributions of the volumetric entropy generation rates due to chemical reaction, heat dissipation and mass transport, respectively. The entropy generation due to chemical reaction shows that the peak value of the volumetric rate of entropy generation due to chemical reaction is less at zero gravity than at normal gravity (Fig. 7(a)). This indicates that the flame is less intense at zero gravity condition than that at normal gravity. The reason may be attributed to the fact that at normal gravity due to high rate of entrainment of flow, oxygen will be carried from the co-flow into the flame zone at a faster rate. In the absence of such high entrainment rate

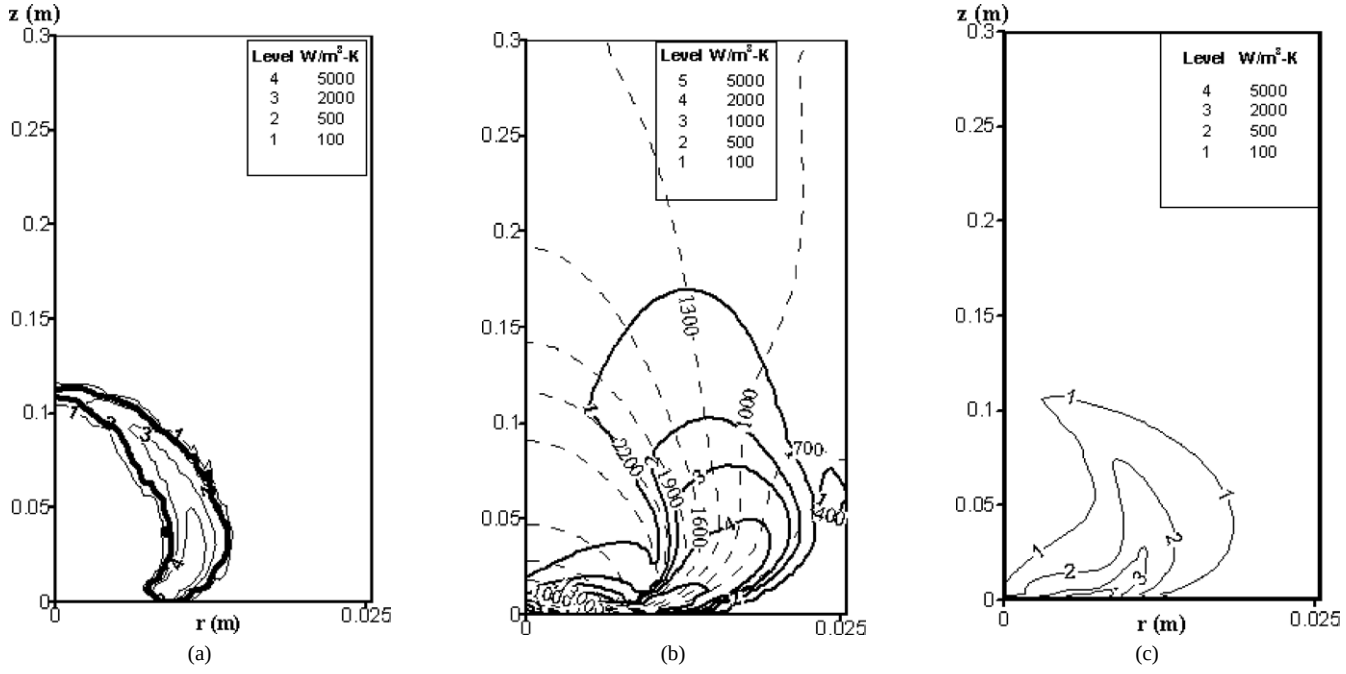

Fig. 7. (a) Flame front (thick line)and distribution of volumetric rate of entropy generation due to chemical reaction (solid contours) at zero gravity. (b) Temperature (in K) distribution (dotted contours) and the distribution of volumetric rate of entropy generation due to heat dissipation (solid contours) at zero gravity. (c) Distribution of volumetric rate of entropy generation due to mass transfer at zero gravity. The box insert in Fig. 7(a)–(c) show the values of the contour levels for the volumetric entropy generation rate.

from the co-flow, the intensity of the flame reduces at zero gravity. However, the total rate of entropy generation due to chemical reaction is not much different at the two different gravity levels, which is shown later. This is because the volume of the flame front at zero gravity level is more due to the increased width of the flame. The higher volume of the flame front compensates the decrease in the volumetric entropy generation rate that takes place at zero gravity.

Fig. 7(b) reports the plot for volumetric entropy generation rate due to heat dissipation at zero gravity along with the respective temperature distribution. Comparing the figure with Fig. 6(b) for normal gravity, it can be seen that the maximum volumetric entropy generation rate is similar in both the cases. However, in absence of buoyancy, the flow structure is such that heat dissipation from the flame into the surroundings takes place more readily. The thermal stratification in the flow is not observed and there is no ingress of fluid from the exit. As a result, the radial temperature distribution is much uniform beyond a certain height above the burner and the entropy generation is low. Thus the volume over which high entropy generation takes place as a result of heat dissipation is diminished. This decreases the entropy generation rate due to heat dissipation at zero gravity.

The entropy generation due to mass transport takes place around the flame zone (Fig. 7(c)). There is not much difference in the nature of this result from the corresponding result at normal gravity shown earlier. The magnitude of the rate of entropy generation due to mass transfer is low in most of the zone of interest. A high rate is again observed only above the entry plane and at the interface of the two jets.

Fig. 8 shows a plot of the total rate of entropy generation in the confined domain and the rate of entropy generation due to individual processes in diffusion flame at various gravity levels. The entropy generation due to fluid friction is not included in the figure due to its very low value. It is seen that out of all the individual processes, the most dominant role towards entropy generation in diffusion flame is played by heat dissipation under all gravity conditions. Chemical reaction is the next significant contributor and mass transfer comes as third important. With the change in gravity level, the entropy generation due to reaction and mass transfer hardly changes in magnitude. However, the entropy generation due to heat transfer is grossly affected by gravity. It is already explained from Figs. 6(b) and 7(b) that as the gravity level is reduced the temperature field becomes more uniform and the entropy generation due to heat dissipation decreases. This decrease in the entropy generation is also reflected in the total entropy generation rate and results in a decrease in the total entropy generation.

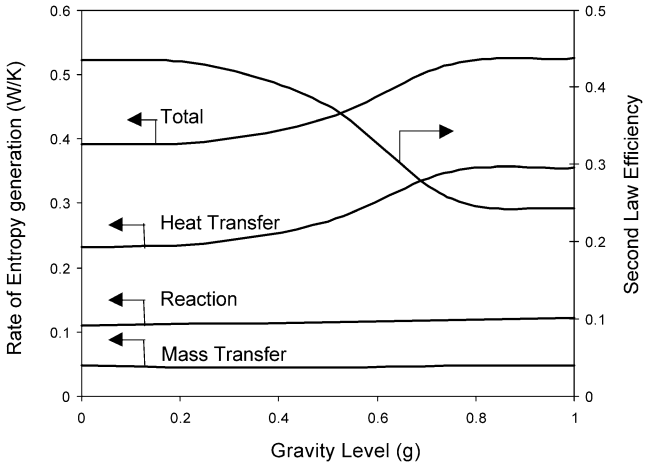

Fig. 8. Variation of the rate of entropy generation (total as well as for individual processes) and Second Law Efficiency in a confined laminar diffusion flame at different gravity levels.

Therefore, it is evident that the gravity in earth's atmosphere has got a significant influence on the entropy generation and irreversibilities in diffusion flames within a confined domain. The influence is sensed by the change in the flow pattern caused by the buoyancy effect. Due to buoyancy a strong thermal stratification takes place in the flow, which generates high rate of heat dissipation. Buoyancy does not influence the contribution of chemical reaction towards entropy generation. The relatively higher rate of combustion and resulting higher volumetric rate of entropy generation is compensated by the thinner flame at normal gravity.

The incoming exergy into the confined domain is due to fuel only, as air is supplied at exergy reference temperature. The fuel flow rate and fuel temperature being the same for all the cases of different gravity, the incoming rate of exergy (A_{in}) remains always the same. The decrease in the entropy generation at micro-gravity condition also decreases the irreversibility of the reacting flow (Eq. (17)) and increases the second law efficiency of the process (Eq. (18)). Fig. 8 also shows a plot of second law efficiency of the diffusion flame in the confined domain for different gravity levels. It is seen that the second law efficiency decreases from 43.5% at zero gravity to 24.2% at normal gravity. The diffusion flame itself is highly irreversible in nature and causes a large loss of exergy. But this loss is much enhanced in presence of the buoyant motion at normal gravity because of the thermal stratification caused by the flow condition. The way to improve the second law efficiency of diffusion flame under earth's atmosphere is to go for conditions where the thermal stratification can be evaded and a uniform distribution of temperature can be obtained.

5. Conclusion

A numerical model is developed for the prediction of a co-flowing laminar jet diffusion flame in an axi-symmetric, confined geometry. The predicted flame parameters are used to evaluate the entropy generation in the confined domain, including the flame front, at various gravity levels. The flame structure is analyzed from the flame shape as well as using the volumetric entropy generation rate data. The following major conclusions can be made:

- It is found that the flame becomes wider at reduced gravity level, but the flame height is affected only marginally. The flame width can be represented in terms of Froude number and burner port diameter as, $w = 2.08 d_f Fr^{0.146}$ at all gravity levels.
- The flame is more intense near its base, where the volumetric rate of entropy generation due to chemical reaction is high. The flame intensity at the base is found to be more at normal gravity than at zero gravity. This is because of the higher rate of air entrainment from the co-flow at normal gravity under the influence of buoyancy.
- The rate of entropy generation due to heat transfer is found to be the maximum in diffusion flames. The second major contributor to the rate of entropy generation is the chemical reaction. Mass transfer is the third most important to this cause and fluid friction produces insignificant amount of entropy compared to the others.
- Gravity has no influence on the rate of entropy generation due to chemical reaction. Though, the flame intensity increases with the gravity level and the resulting volumetric entropy generation rate becomes higher, the decrease in the volume of the flame front compensates it.
- The rate of entropy generation due to heat transfer is very much influenced by gravity. The buoyant motion at normal gravity stratifies the high temperature gas and causes high gradient of temperature in the field. Therefore, the rate of entropy generation due to heat dissipation increases with the gravity level. As a result, the total rate of entropy generation in the confined domain also increases significantly with the gravity.
- The entropy generation due to mass transfer is only significant around the flame zone. However, the volumetric rate is low except just above the burner outlet and at the interface of the two jets. The contribution of mass transfer towards total entropy generation is low and remains almost same at all gravity levels.
- The increase in the total rate of entropy generation with gravity increases the rate of exergy loss inside the confined domain and reduces the second law efficiency of the confined diffusion flame.

References

[1] C.K. Law, G.M. Faeth, Opportunities and challenges of combustion in microgravity, Prog. Energy Combust. Sci. 20 (1994) 65–113.

[2] K.C. Lin, G.M. Faeth, P.B. Sunderland, D.L. Urban, Z.G. Yuan, Shapes of nonbuoyant round luminous hydrocarbon/air laminar jet diffusion flame, Combust. Flame 116 (1999) 415–431.

[3] R.W. Davis, E.F. Moore, R.J. Santoro, J.R. Ness, Isolation of buoyancy effects in jet diffusion flame experiments, Combust. Sci. Technol. 73 (1990) 625–635.

[4] P.B. Sunderland, B.J. Mendelson, Z.G. Yuan, D.L. Urban, Shapes of buoyant and nonbuoyant laminar jet diffusion flames, Combust. Flame 116 (1999) 376–386.

[5] H.D. Ross, R.D. Sotos, J.S. T'ien, Observation of candle flames under various atmospheres in microgravity, Combust. Sci. Technol. 75 (1991) 155–160.

[6] K. Maruta, Y. Masaharu, G. Hongsheng, Y. Ju, T. Niioka, Extinction of low-stretched diffusion flame in microgravity, Combust. Flame 112 (1998) 181–187.

[7] A. Atreya, S. Agrawal, Effect of radiative heat loss on diffusion flames in quiescent microgravity atmosphere, Combust. Flame 115 (1998) 372–382.

[8] O.A. Ezekoye, Z. Zhang, Soot oxidation and agglomeration modeling in a microgravity diffusion flame, Combust. Flame 110 (1997) 127–139.

[9] J.H. Keenan, A system chart for second law analysis, ASME Mech. Engrg. 54 (1932) 195.

[10] A. Bejan, Advanced Engineering Thermodynamics, Wiley, New York, 1988.

[11] V.S. Arpaci, A. Selamet, Entropy production in flames, Combust. Flame 73 (1988) 251–259.

[12] J.Y. San, W.M. Worek, Z. Lavan, Entropy generation in convective heat transfer and isothermal convective mass transfer, J. Heat Transfer Trans. ASME 109 (1987) 647–652.

[13] J.O. Hirschfelder, C.F. Curtiss, R.B. Bird, Molecular Theory of Gases and Liquids, Wiley, New York, 1954.

[14] I.K. Puri, Second law analysis of convective droplet burning, Internat. J. Heat Mass Transfer 35 (10) (1992) 2571–2578.

[15] S. Hiwase, A. Datta, S.K. Som, Entropy balance and exergy analysis in the process of droplet combustion, J. Phys. D: Appl. Phys. 31 (1998) 1601–1610.

[16] A. Datta, S.K. Som, Thermodynamic irreversibilities and second law analysis in a spray combustion process, Combust. Sci. Technol. 142 (1999) 29–54.

[17] A. Datta, Entropy generation in a confined laminar diffusion flame, Combust. Sci. Technol. 159 (2000) 39–56.

[18] K. Nishida, T. Takagi, S. Kinoshita, Analysis of entropy generation and exergy loss during combustion, in: Proc. of the 29th Symp. (Int.) of the Combustion Inst., vol. 29, 2002, pp. 869–874.

[19] R.E. Mitchell, A.F. Sarofim, L.A. Clomburg, Experimental and numerical investigation of confined laminar diffusion flames, Combust. Flame 37 (1980) 227.

[20] M.D. Smooke, R.E. Mitchell, D.E. Keyes, Numerical solutions of two-dimensional axisymmetric laminar diffusion flames, Combust. Sci. Technol. 67 (1989) 85–122.

[21] V. DuPont, M. Pourkashanian, A. Williams, Modeling of process heaters fired by natural gas, J. Inst. Energy 73 (1993) 20–27.

[22] V.R. Katta, L.P. Goss, W.M. Roquemore, Effect of nonunity Lewis number and finite rate chemistry on the dynamics of a hydrogen–air jet diffusion flame, Combust. Flame 96 (1994) 60.

[23] R.C. Reid, J.M. Prausnitz, B.E. Poling, The Properties of Gases & Liquids, fourth ed., McGraw-Hill, New York, 1988.

[24] S.R. Turns, An Introduction to Combustion, McGraw-Hill, New York, 1996.

[25] C.G. Carrington, Z.F. Sun, Second law analysis of combined heat and mass transfer phenomena, Internat. J. Heat Mass Transfer 34 (11) (1991) 2767–2773.

[26] C.W. Hirt, J.L. Cook, Calculating three-dimensional flows around structures and over rough terrain, J. Comput. Phys. 10 (1972) 324–341.